SAND2013-9173J

Modeling infrasound signal generation of an underground explosion at the Source Physics Experiment using the Rayleigh integral

Kyle R. Jones[1], Rodney W. Whitaker[2], and Stephen J. Arrowsmith[2]
[1] Sandia National Laboratories, NM, USA. E-mail: krjones@sandia.gov
[2] Los Alamos National Laboratory, NM, USA.

Accepted date. Received date; in original form date

Abbreviated Title: Infrasound modeling using the Rayleigh integral

Kyle R. Jones

Sandia National Laboratories

P.O. Box 5800

Albuquerque, NM 87185-0404, USA

Phone: 505-285-2621

Fax: 505-844-5321

Email: krjones@sandia.gov

SUMMARY

The overall mission of the Source Physics Experiment (SPE) is to improve upon and develop new physics-based models for underground nuclear explosions using scaled, underground chemical explosions as proxies. To this end, we use the Rayleigh integral as an approximation to the Helmholtz-Kirchoff integral to model infrasound generation and propagation in the far-field. Infrasound generated by single-point explosive sources above ground can typically be treated as monopole point sources. While the infrasonic source is relatively simple, the research needed to model infrasound from above ground point sources is complicated by path effects related to the propagation of the acoustic signal and

out of the scope of this study. In contrast, for explosions that occur below ground, including the SPE explosions, the source region is more complicated but the observation distances, considered here, are much closer (< 5km), thus greatly reducing the complication of path effects. In this case, elastic energy from the explosion radiates upward and spreads out, depending on depth, to a more distributed region at the surface that couples to the atmosphere. Due to this broad surface perturbation of the atmosphere, we cannot model the infrasonic source as a simple monopole point source. Instead, at the surface, we can invoke the analogy of a piston mounted in a rigid, infinite baffle, where the surface area that moves as a result of the explosion is the piston and the surrounding region is the baffle. The area of the piston is determined by the depth, explosive yield, and underlying geologic structure. In this study, we look at the second explosion from SPE (SPE-2). This shot had an explosive yield of 997.45 kg at a depth of 45.7 m. We collected infrasound data using seven arrays of 28 sensors within a 5 km radius of ground zero. To determine the area of the surface acceleration, we used data from twelve surface accelerometers installed within 100 m radially around ground zero. With the accelerometer data defining the vertical motion of the surface, we use the Rayleigh integral to generate synthetic infrasound traces to compare to the observed data. This method produces reasonable synthetic pulses that are similar in overall shape to the observed data with minor structural differences potentially due to topography, meteorological conditions, and assumptions made about the source region. We also applied a two-dimensional time-domain, finite difference computational hydrodynamics code to calculate the atmospheric infrasound signal in a 2 km by 2 km (range/altitude) domain as an independent way to verify the results of the Rayleigh integral.

Key Words: Acoustic properties; Infrasound; Time series Analysis; Numerical approximations and analysis; Controlled source seismology; Seismic monitoring and verification; Wave propagation

INTRODUCTION

The goal of the Source Physics Experiment (SPE) is to improve upon and develop new physics-based models for underground nuclear explosion monitoring. An important aspect of this goal is the ability to utilize not only seismic, but infrasound data to further our understanding of underground explosions and event discrimination. Typically, infrasound observations for nuclear explosion monitoring are made at great distances away from a source (Christie & Campus 2010). At these distances the character of the signal has changed dramatically and it can be difficult to determine the near-field characteristics of the source (Szuberla et al. 2006). Unlike traditional seismology, the medium through which infrasound waves propagate changes dynamically over very short time scales (Evers et al. 2012). SPE allows us to observe the infrasound generated from the surface ground motion of an underground explosive source at very close range (.25 to 5 km), effectively reducing propagation effects such as wind and regional topography.

The challenging aspect of this series of experiments is that they are not simple, above ground sources, but instead are over-buried (with respect to traditional underground nuclear testing practice), seismically well-coupled events that interact with the atmosphere in potentially complicated ways due to geology, ground saturation, fracturing from previous explosions, etc. Using data from vertical accelerometers installed azimuthally around ground zero, we use the Rayleigh integral to produce synthetic infrasound

waveforms that can be directly compared to the observed waveforms and to waveforms produced by other models to explore and determine if changes in the source region can be detected using infrasound.

The second explosive test in the SPE (SPE-2) series was conducted on October 25, 2011 at 19:00 UTC. The shot consisted of 997.45 kg [~1 ton TNT equivalent] Sensitized Heavy Ammonium Nitrate and Fuel Oil (SHANFO) buried to a depth of 45.7 m, scaled depth of burial (SDOB) of ~363 m, (Snelson et al. 2013). This paper will focus only on the recorded observations from the second SPE test as well as the efforts to model the source using the Rayleigh integral with a short discussion and a path forward.

Network of Infrasound Arrays

Prior to the SPE-2 shot, seven arrays consisting of four Inter-Mountain Labs (IML-ST) infrasound sensors were deployed around ground zero. The data were recorded using Reftek RT-130 digitizers sampling at 500 Hz. Each station telemetered data in real-time to the Sandia trailer at the command center ~365 m southeast of ground zero (Fig. 1).

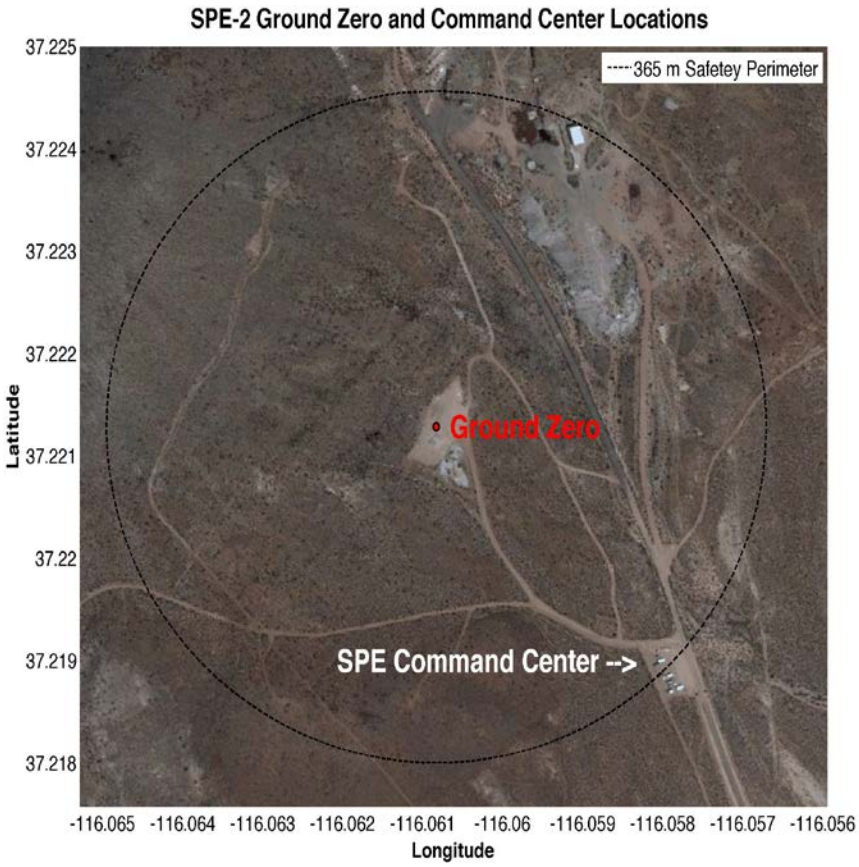

Figure 1. Map showing the locations of ground zero in relation to the SPE command center. Dashed line indicates the 365 m safety perimeter during the time of the shot.

The infrasound sensors were installed in a roughly triangular geometry with one sensor and the digitizer at the center and the other three sensors arranged azimuthally (~120° increments) around the center element at a distance of ~30 m. Attached to each sensor were four lengths of ~15 m porous hoses for wind noise reduction. The IML-ST sensors have a nominal sensitivity of 0.20 V/Pa and a flat response from 30 Hz down to where the roll-off begins around 2 Hz (Hart, 2007). For this reason, we remove the instrument response from the data prior to processing. Four arrays were installed azimuthally around the explosives pad approximately 0.25 km from ground zero at different elevations due to

topography constrains. The remaining three arrays were located at 1, 2 and 5 km respectively linearly south-southeast of ground zero (Fig. 2).

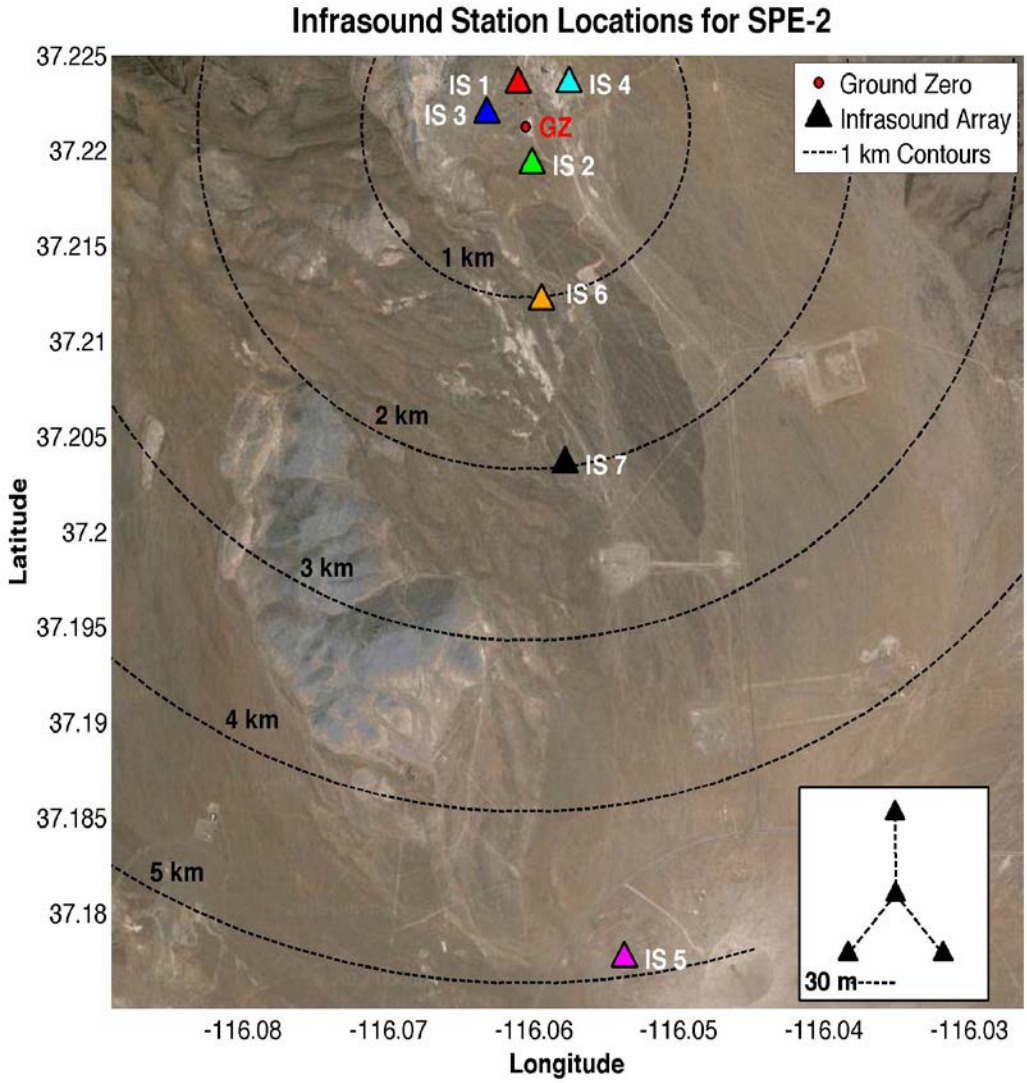

Figure 2. Map showing the seven infrasound array locations (triangles) around ground zero (red) used for SPE-2. Dashed lines are 1 km contours from ground zero for scale. Inset shows an example of the sensor geometry at each array. Array station colors correspond to the amplitudes at each array in Fig. 7.

The surface acceleration data (discussed in detail in a later section) were recorded using twelve Endevco 500g vertical accelerometers installed in a "cross" geometry above ground zero (Fig. 3). Two accelerometers were installed to the north, east and west with the remaining six linearly spaced to the south-southwest. The geometry of the sensors was predetermined by the space constraints of explosive pad and surrounding topography.

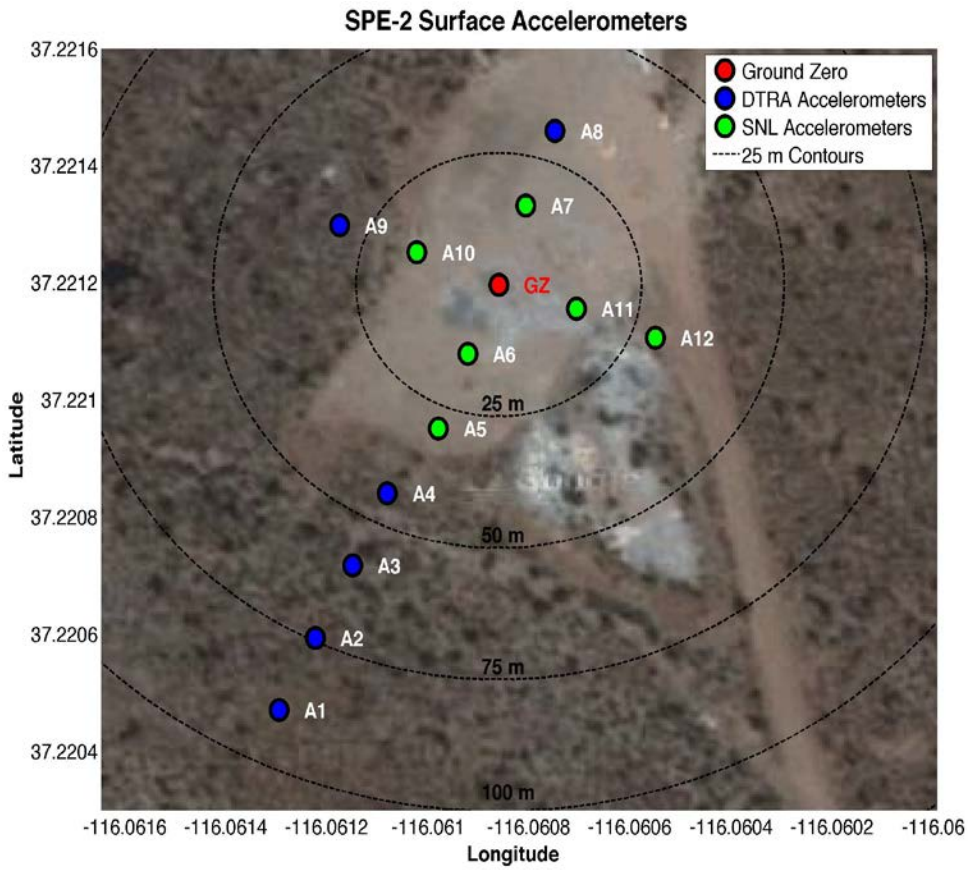

Figure 3. Map of ground zero (red) and surrounding instrument pad showing the locations of twelve Endevco 500g vertical surface accelerometers installed by Sandia (green) and DTRA (blue). The dashed lines represent distances of 25 m from ground zero.

Data Observations

The ground-motion-generated acoustic wave propagated across the entire network with zero-to-peak amplitudes from ~16.4 Pa at the closest stations to less than 0.2 Pa at 5 km. The waveforms exhibit a shape that is asymmetric due to phase differences in the source, the off-axis location of the arrays (Fig. 4), and filtering. We will discuss on-axis vs. off-axis pressures and other causes of waveform variability in later sections.

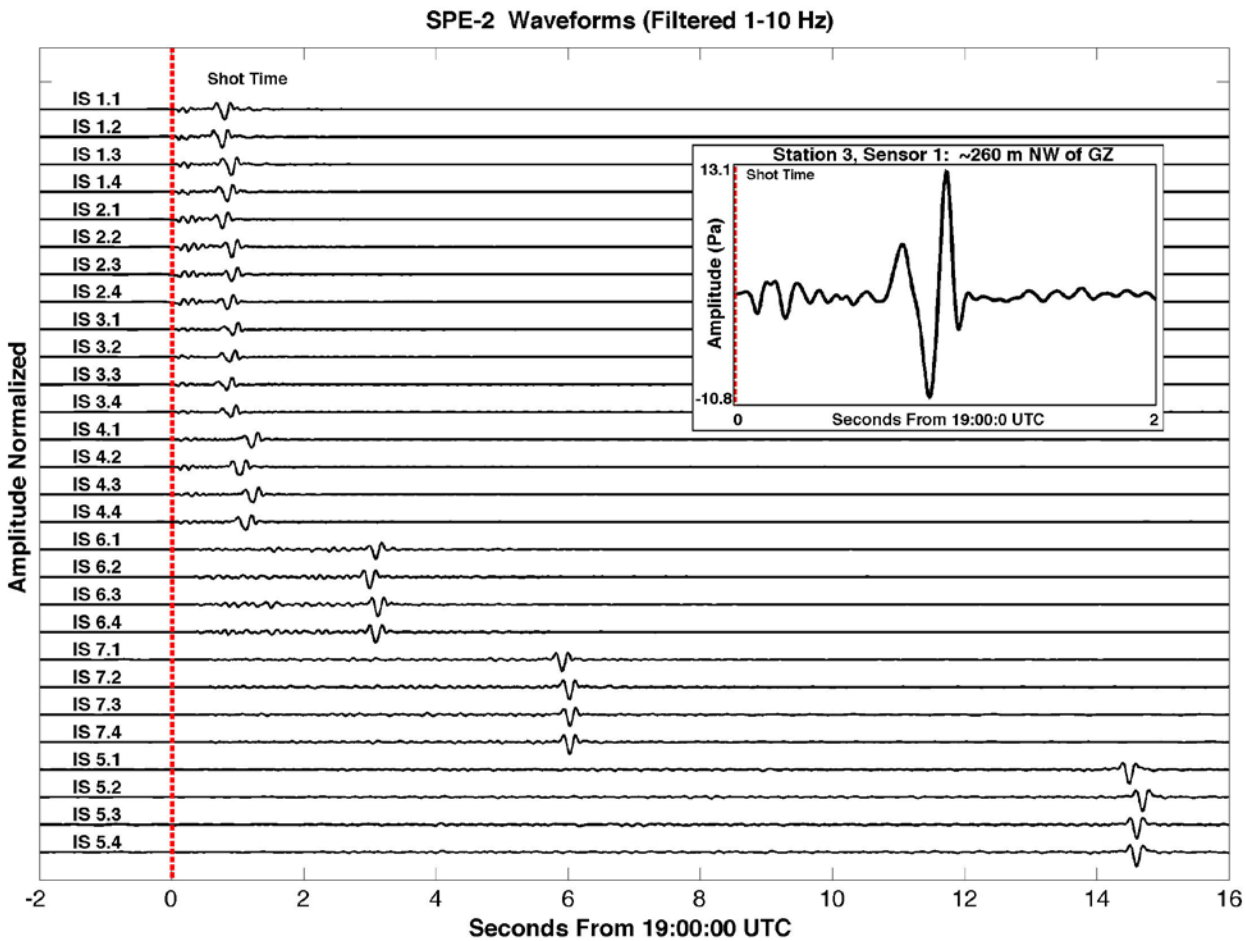

Figure 4. Waveforms for each sensor arranged according to distance and bandpass filtered between 1 and 10 Hz. The explosion propagated across the entire network out to 5 km. The Inset shows an example waveform from station 3, sensor 1.

The Rayleigh Integral

The Rayleigh integral (RI) allows for the calculation of pressure as a function of time at an arbitrary observation point above an area that has a known acceleration history as a function of time and position. The observation point can be on or off the vertical axis of the ground motion area. Banister (1979), presented an earlier application of the RI to the calculation of near-field, atmospheric pressure signals generated by the surface ground motion from underground nuclear tests. While our work is similar to Banister's, we apply this method to a much smaller source. This method has also been used by Whitaker (2007, 2008, 2009) for modeling infrasound generated from underground nuclear explosions (UGTs) and more recently, the RI has been successfully used to model epicentral infrasound from the M_w 4.7 Circleville earthquake in Utah in January 2011 (Arrowsmith et al., 2012).

Formally, the RI provides a means to calculate the pressure generated by an area of surface acceleration as in Eq. I

$$p(x,y,z;t) = \rho_0 \int_S \frac{\dot{u}\left(x',y';t-\frac{R}{c_0}\right)}{2\pi R}\, dS, \qquad \text{(I)}$$

where p is a function of x, y, z and time, ρ_0 is the density of air, c_0 is the speed of sound in air, $\dot{u}$ is the piston acceleration, x', y' are the coordinates of each source point on the area dS of the piston, and R is the distance from the point x', y' to the observation point (Blackstock, 2000). Fig. 5 shows the geometry used in the RI.

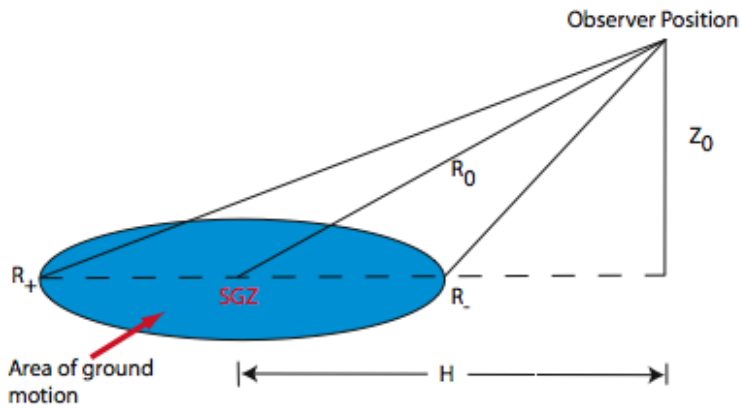

Figure 5. Illustration of the observer parameters in the Rayleigh integral technique. SGZ is the surface ground zero at the center of the ground motion; R_+ and R_- indicate the extent of motion. The observer is at a horizontal distance H from SGZ and vertical distance Z_0 above SGZ, at a slant range of R_0**.**

For the application of the RI to the calculation of near-field infrasound signals, from underground explosions, the source of the surface ground motion is the upward propagating stress/elastic wave. Acceleration amplitudes are generally largest at surface ground zero and decay radially outward with distance. When the elastic wave reaches the surface, there is vertical ground motion that drives a signal in the atmosphere. This can be visualized as a piston mounted in an infinite, rigid baffle, where the piston, in reality, is not completely rigid.

For large sources, the ground may be driven into tensile failure (spall) that is seen as a -1g acceleration piece of the acceleration versus time history (Fig. 6).

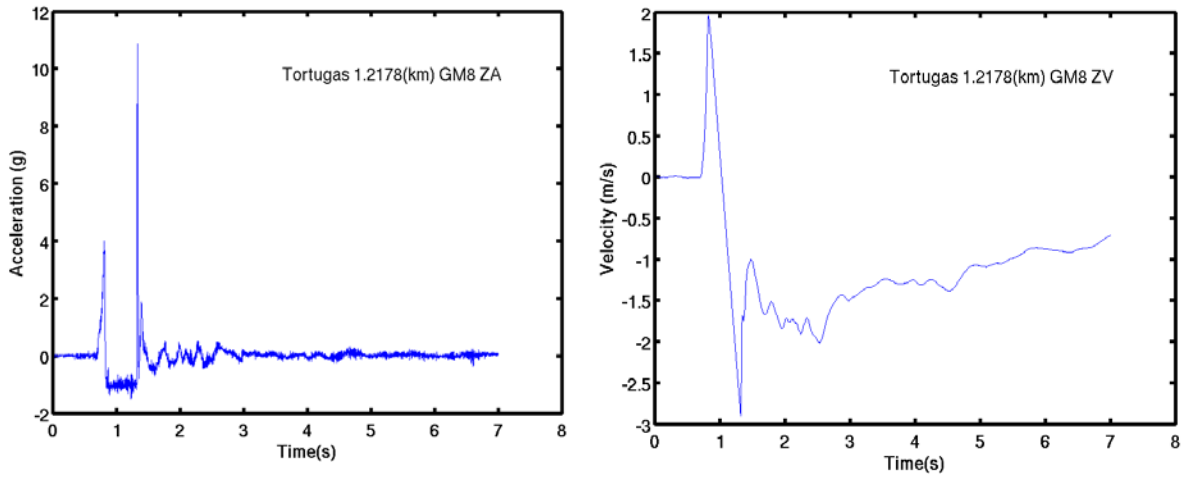

Figure 6. A measured ground motion acceleration record for Totugas (left) and the velocity record (right) where units are gs for acceleration and m/s for velocity. The spall phase is seen in the acceleration record at 1 second.

The acceleration records for SPE-2 show spall as well (Fig. 8). While spall is an important contributor to the near-field infrasound signal, vertical ground motion without spall can still generate an atmospheric signal, as demonstrated by earthquake-generated infrasound. In the simple parabola model for the surface acceleration, the peak velocity determines the ground motion after the initial acceleration pulse (Lee & Walker 1980). From this, the peak velocity is at the time the acceleration goes to zero and the duration of spall is just the ballistic free-fall time from that velocity peak. In this model, with peak acceleration A and width w, it can be shown that the peak velocity is

$$V_{pk} = \frac{2Aw}{3}, \tag{II}$$

the vertical displacement at this time is

$$d = \frac{Aw^2}{3}, \tag{III}$$

and the maximum displacement is when the velocity crosses zero and is given by

$$d_{pk} = \frac{Aw^2}{3} + \frac{V^2{}_{pk}}{2g}, \tag{IV}$$

where g is the acceleration of gravity.

Another useful analytic expression can be derived for a uniform piston of radius R with sinusoidal displacement amplitude A, at frequency f. One can show that the on axis peak pressure, p, at height h, is given by,

$$p = \frac{2\pi^2 A\rho f^2 R^2}{h} \tag{V}$$

where ρ is the air density.

Source Physics Experiment Data Analysis

Using the observed data, we plot the filtered overpressure amplitudes (zero-to-peak) for each sensor with distance and fit a $\frac{1}{r^{1.1}}$ and standard $\frac{1}{r}$ decay line to the data (ANSI 1983) (Fig. 7). While the data generally fit the decay lines, there is some variability both in the overall trend and within each array. We attribute the close-in station amplitude differences to the elevation variability between the arrays, topography at each sensor, and the degree of on-axis pressure each array is observing. The overall trend deviates at ~1 km such that the amplitudes are less than both decay lines. We believe this can be attributed to

topography, wave refraction, and/or a directionality component preventing the wave from propagating uniformly due to a north-northeast prevailing wind during the shot.

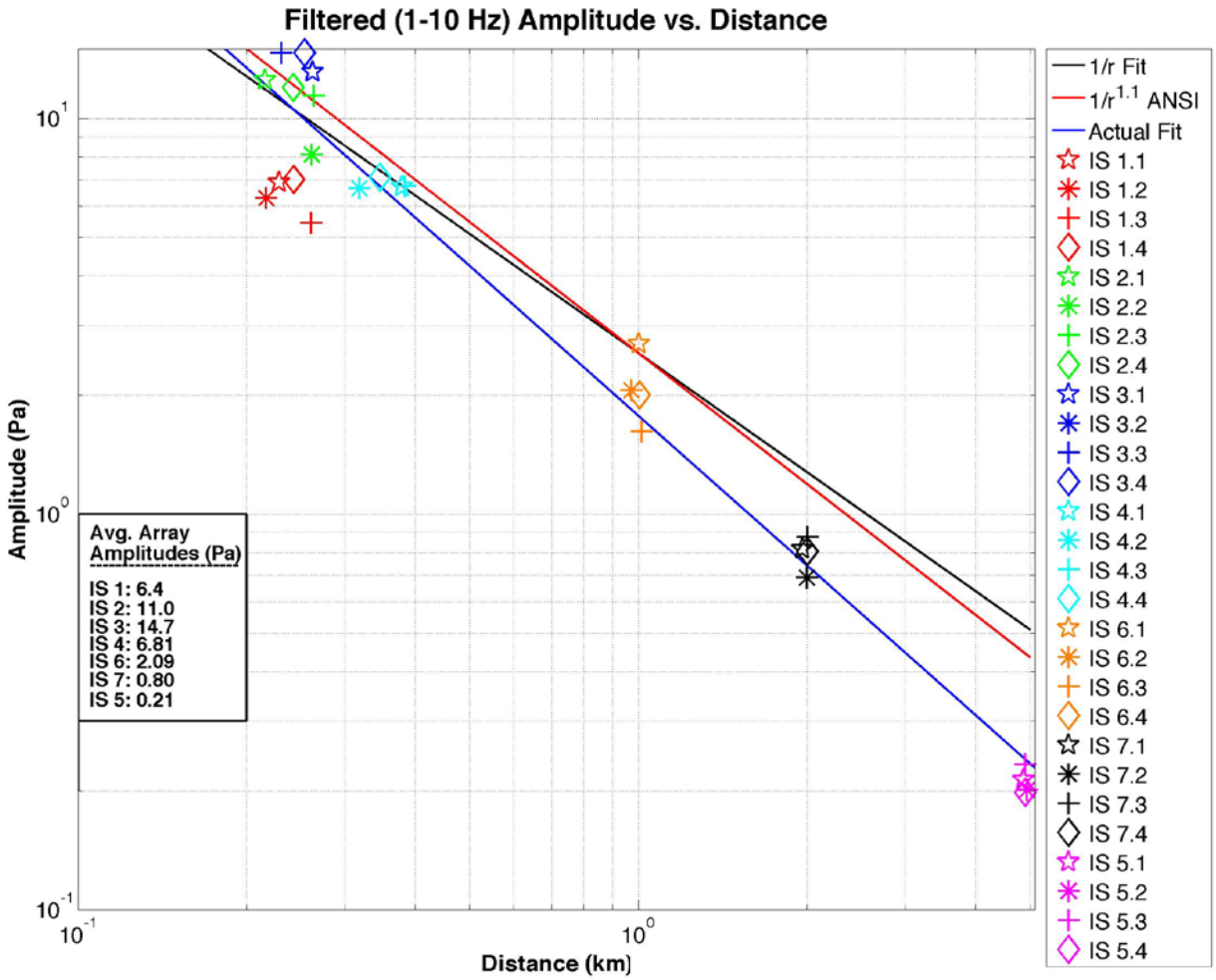

Figure 7. Filtered amplitude vs. distance for each array sensor. The data were fit with an ANSI $\frac{1}{r^{1.1}}$ and standard $\frac{1}{r}$ amplitude decay rate. Neither decay rate fits the data perfectly and can be attributed to north-northeast winds and or topography. Inset table shows the average filtered peak amplitude at each array. "IS N.M" represents infrasound array N station M.

Vertical Surface Accelerations as a Source

To model the source we use a 200 m square grid (for simplicity) with ground zero at the center. The Defense Threat Reduction Agency (DTRA) and Sandia National Labs (SNL) both used the same brand of accelerometer (ENDEVCO 500 g) to record the surface accelerations. DTRA sampled at a rate of 1,000,000 SPS and SNL used 4,000 Hz. The DTRA data were down-sampled by a factor of 1,000 and the SNL data by a factor of 4 so that both datasets matched at 1000 Hz for use in our analysis (Fig. 8).

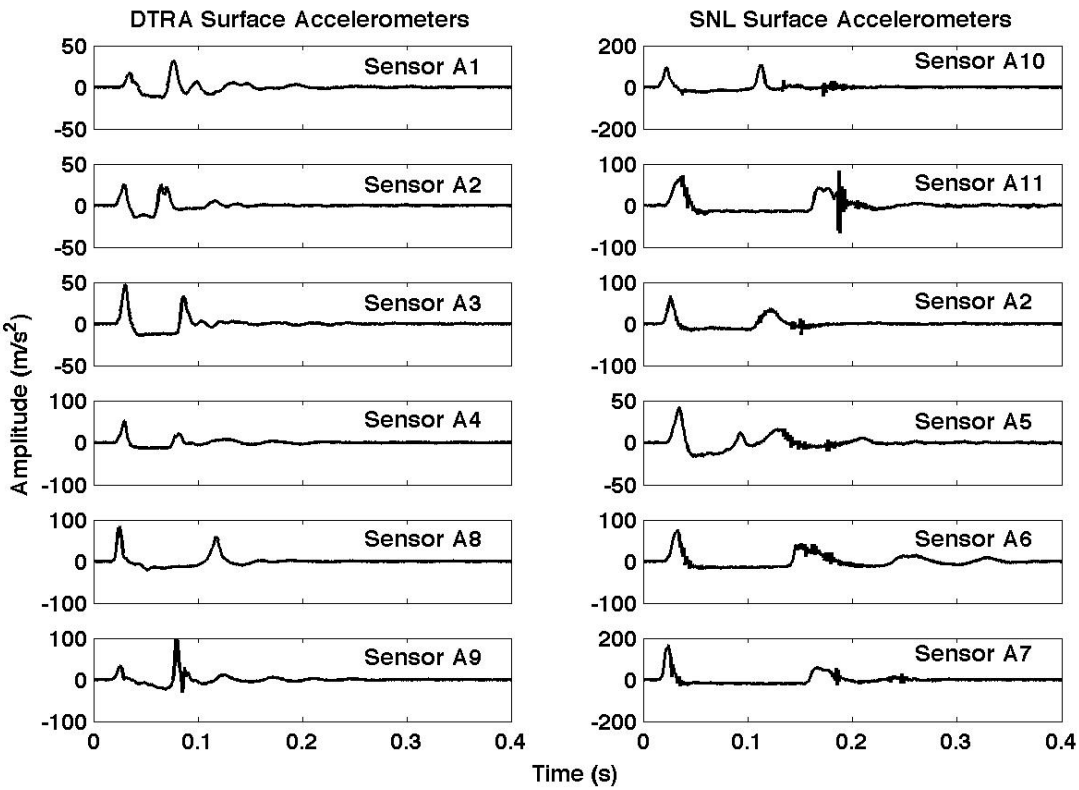

Figure 8. DTRA and SNL unfiltered surface accelerometer records out to 0.4 seconds. See Fig. 3 for sensor location.

As applied to SPE-2, the (RI) uses the vertical accelerations recorded at the twelve surface accelerometers located at surface ground zero. The area, dS, is divided into uniform square sections to form a grid approximately the size of the area of uplift. The acceleration in each

elemental area (dS) was defined by interpolating and extrapolating the accelerations observed by the twelve accelerometers for each sample in time from 0 to 0.4 seconds over the entire grid area. To do this, we needed to find a way to both interpolate and extrapolate the grid using only twelve sparse data points. Attempting to use the built-in Matlab© functions for linear, cubic spline and quadratic interpolation/extrapolation resulted in artifacts that were "non-physical" and caused the synthetic infrasound waveform to be unrealistic. Specifically, the synthetic waveform was dominated by a very low frequency component not observed in the actual data. Further investigation found that this was due to a "rocking" or "tilting" of the grid during the extrapolation process. We solved these issues by using radial base functions (RBF) as described by Morse et al. (2005) and using code developed by Alex Chirokov (2006) to interpolate over a non-uniform, sparse data set (Fig. 9).

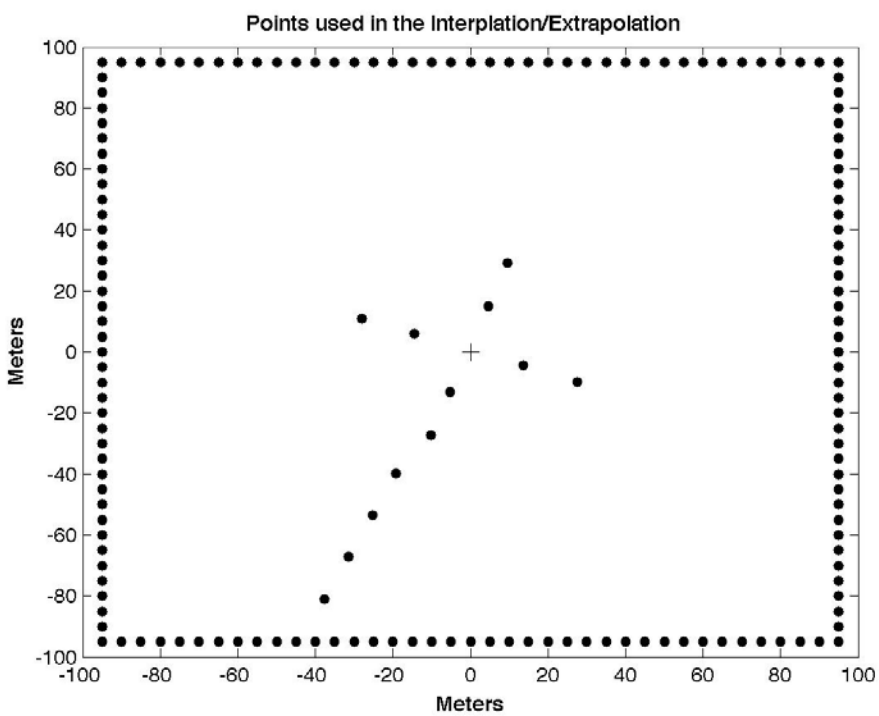

Figure 9. Points used in the interpolation/extrapolation process, including the accelerometers (cross) around ground zero (+) and the fixed points (surrounding box) that were used to reduce the extrapolation artifacts. The interpolation/extrapolation was done using Radial Base Functions, which support a non-uniform, scattered data set.

We also "pinned" the edges of the grid to zero to simulate the edges of the surface source region, which, in reality, are not detached from the surrounding area. We felt that this was an appropriate measure to ensure a more realistic result. As an example, Fig. 10 shows the entire extrapolated grid at time 0.025 seconds after detonation, corresponding to the maximum acceleration. In this case the maximum-recorded acceleration does not occur exactly above ground zero, resulting in an asymmetric surface acceleration, which will be addressed in further detail in the discussion section.

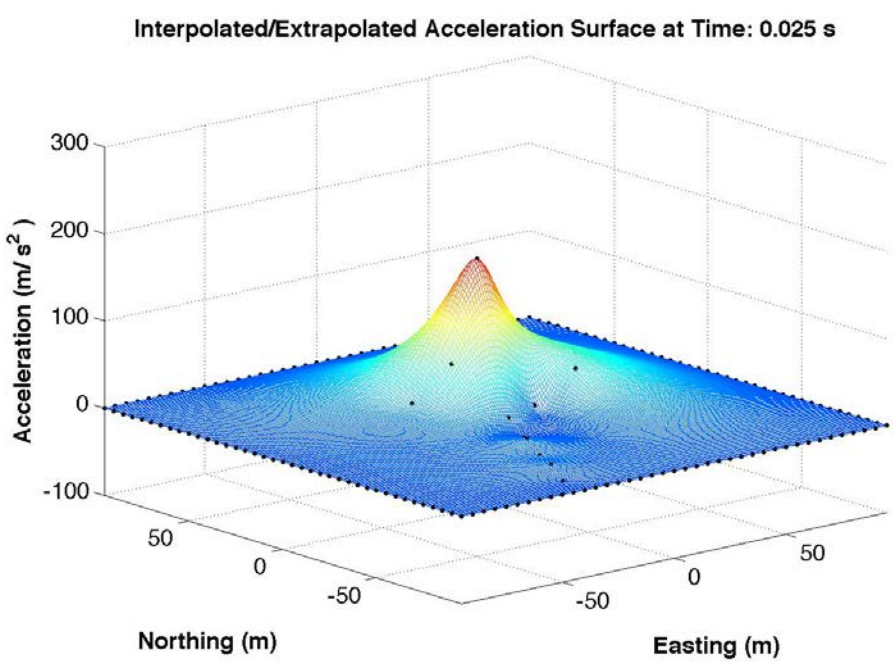

Figure 10. Interpolated and extrapolated surface showing the maximum acceleration at time 0.025 seconds after detonation. Note that the area of maximum acceleration is not centered on the grid, resulting in an asymmetric source.

Comparing observed and synthetic waveforms

Using the Rayleigh integral to generate synthetic waveforms, we compared each station's observed data to a set of synthetic waveforms corresponding to the same distances. We found that, to first order, the synthetic waveforms correlated well with the observed data for time delay, amplitude, and overall waveform shape. This did not hold true for each and every station comparison. For example, the 5 km station showed a phase shift where the synthetic trace shows an arrival before the observed arrival. The time delay could be attributed topography or wind, which the model does not account for. At the distance of 5 km, topography would have a minimal effect on the travel time such that the difference can, most likely, be attributed to wind. At the time of the test there was a 6 m/s wind from the south acting directly against the southward propagation of the pressure wave, resulting in a time delay of ~0.25 seconds. For simplicity and for later data comparison, we use cross-correlation to align the synthetic waveform with the corresponding observed waveform. All of the waveform comparisons are shown in Fig. 11.

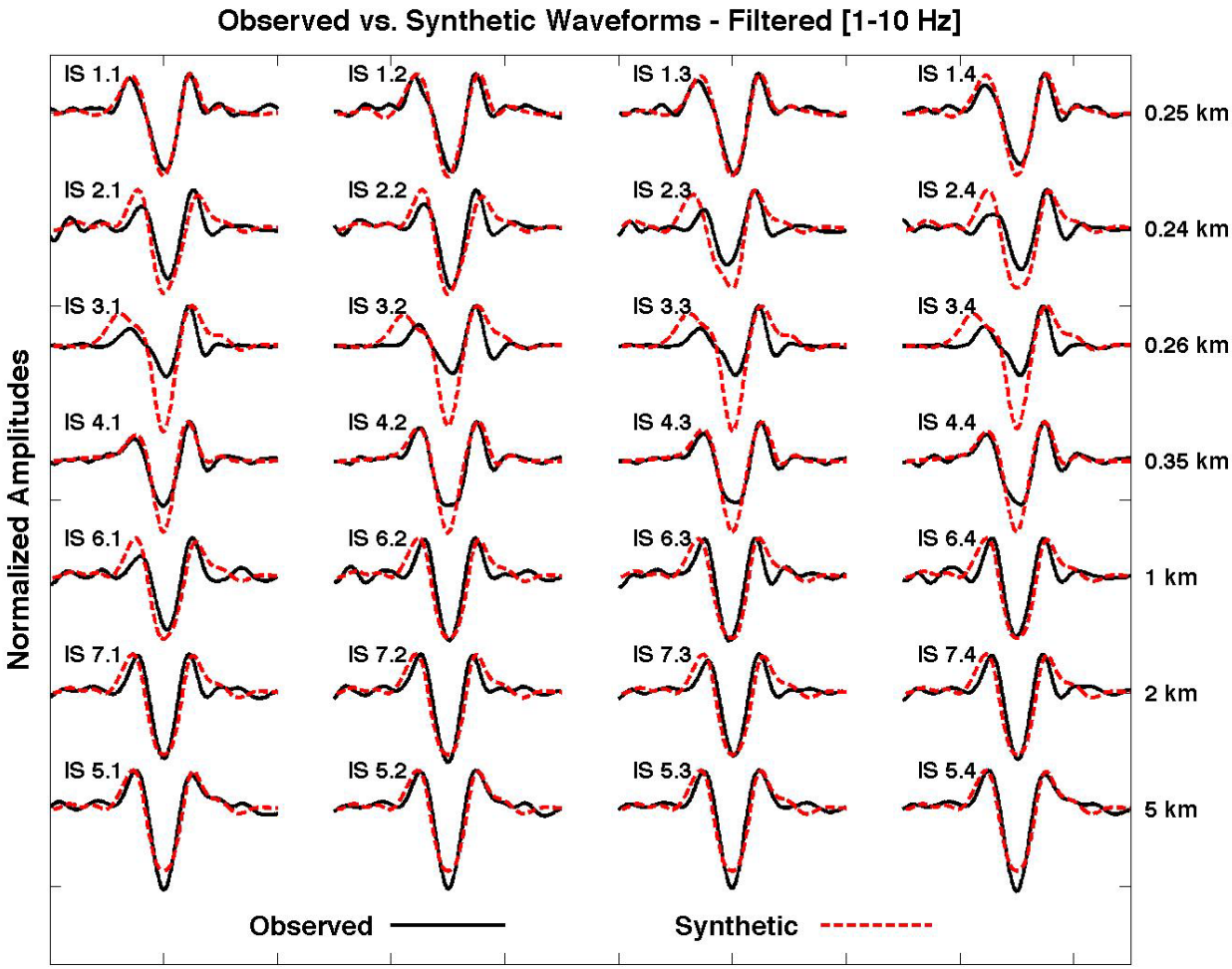

Figure 11. Synthetic pressure traces produced by the Rayleigh integral (dashed red line) compared to the observed data (solid black line) shown for all sensors in the array network. For the sensors at arrays 1, 6, 7, and 5 the overall waveform shape is reproduced very well. Note: "IS N.M" represents infrasound array N station M.

Overall, the shape and amplitude of the synthetic waveforms fit the observed data very well. In particular, arrays 1, 6, 7 and 5 visually show a high degree of correlation in shape and amplitude and in all cases, the period matches well. The variability seems to occur

primarily in the side lobes and in the main trough and could be related to a number of circumstances that our simplistic model doesn't account for. The RI is primarily intended for far-field calculations well above the source. We are testing the limits of this method by calculating waveforms at close range with little to no vertical relief. However, with the results shown above, the RI accurately reproduces the observed waveforms. Additionally, there could be "micro-scale" topography variability, unaccounted for by our method, in which, the sensors at each array are not planar relative to one another. For example, for the close-in arrays, there was limited room for the spatial extent of the installation causing several of the sensors to be installed behind a small rise or significantly lower/higher than the rest of the array. Another potential source of variability can be attributed to the porous hose wind filter system installed on each sensor. When the porous hoses are left out for multiple deployments, the sun breaks down the hose material, which causes signal amplification when compared to data from sensors with new porous hoses. This was observed during the SPE-3 experiment and will be reported on in a future publication.

Observed asymmetry and modeling of the source region

While plotting the acceleration surfaces, we noticed that the area of uplift due to the explosion is not uniform around surface ground zero. We believe this could be due to one or more types of variations in site characteristics. One factor could be differential offset along natural fracture sets present throughout the granite body. Another possible contributing factor could be variations in the fill material that had been placed on the native granite surface to create a level construction pad; this fill varies in thickness across the pad, generally thickening to the southeast. These or other site factors could contribute

to a differential response of different portions of the construction pad. The resulting pressures waves from the explosion reacted differently in different portions of the pad and excited the surface non-uniformly (Drellack et al. 2011; Drellack et al. 2012). In an attempt to verify that the asymmetry was real and not an artifact of the interpolation/extrapolation process we ran simulations using an azimuthally symmetric synthetic source, generated by taking the southwest accelerometer line and rotating it every ten degrees around ground zero (Fig. 12).

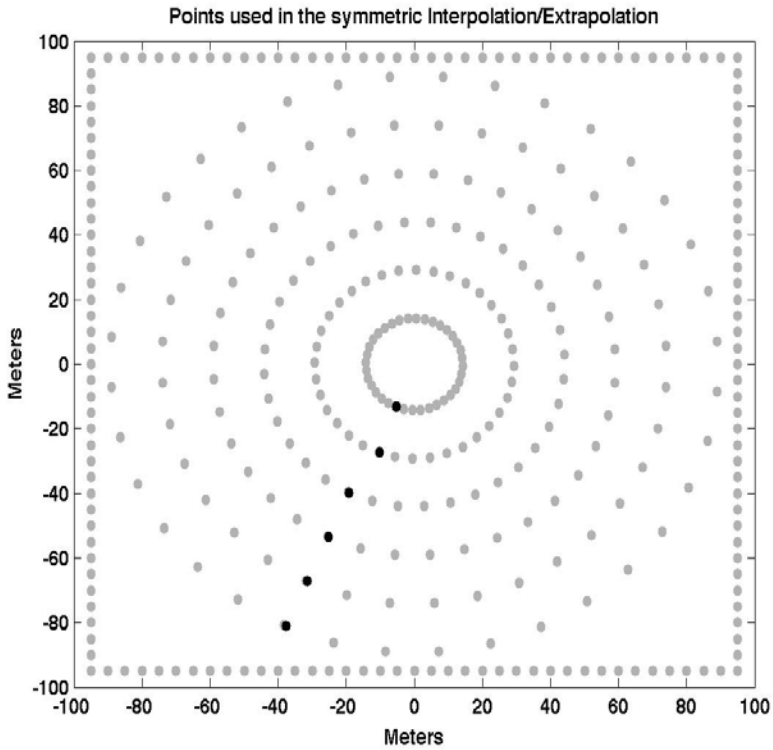

Figure 12. Points used in the azimuthally symmetric interpolation/extrapolation. The black dots are the original accelerometers along the Southwest line and the grey dots are the rotated Southwest line used in the simulation.

After the new acceleration grid was created, we again interpolated/extrapolated and produced synthetic waveforms for each station in the array. Comparisons between the azimuthally symmetric synthetic waveforms and the observed data for the same set of stations are shown in Fig. 13.

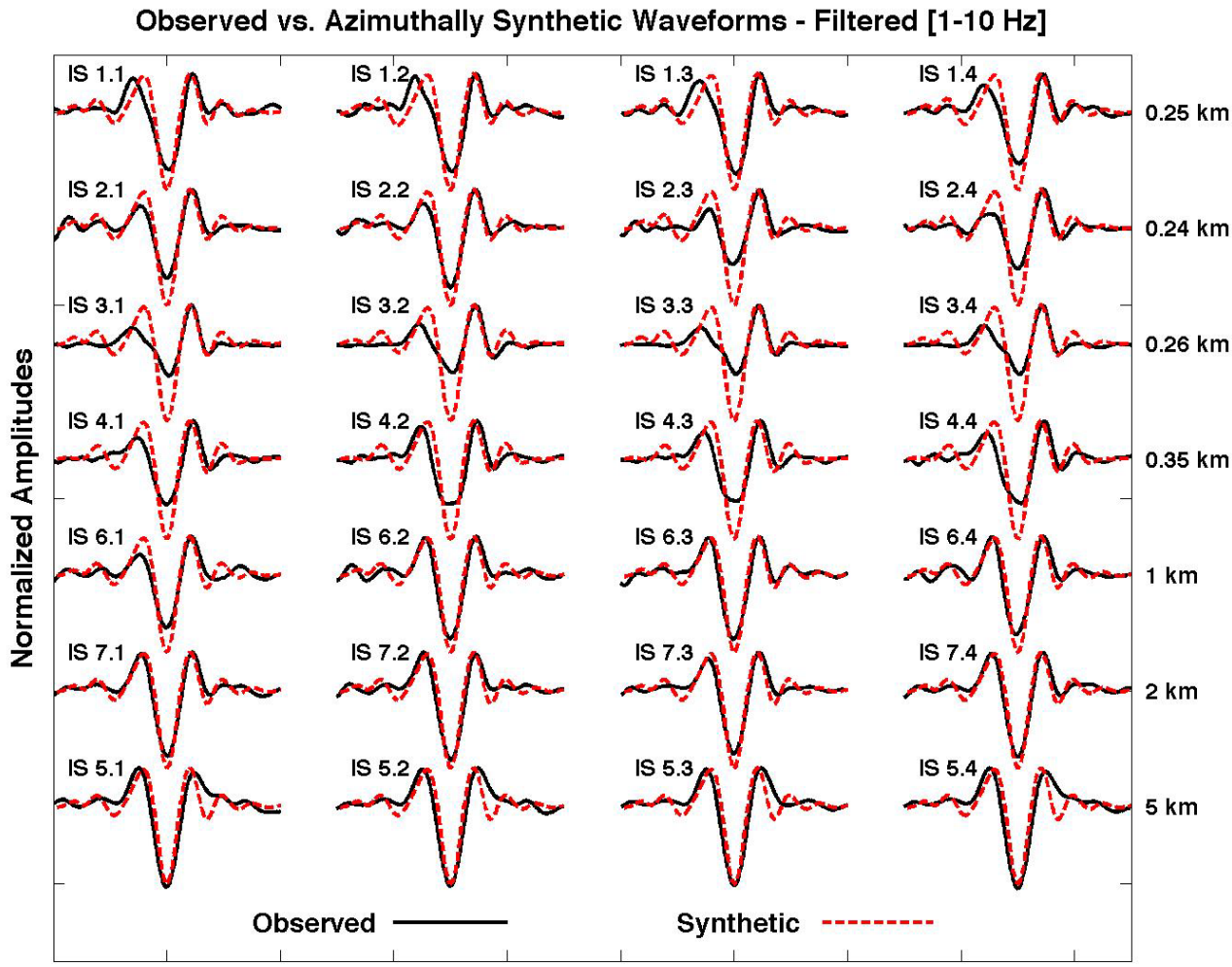

Figure 13. Synthetic pressure traces produced by the Rayleigh integral (dashed red line) using an azimuthally symmetric synthetic source compared to the observed data (solid black lines) for all sensors in the array network.

While comparing the azimuthally symmetric synthetic waveforms to the observed data, two differences are apparent. First, the shape of the waveform is expectedly symmetric. This is to be expected for the type of source we created. Overall, the period of the synthetics visually correlate well to the observed waveforms. However, because the synthetic is symmetric, the waveforms do not achieve the same asymmetric match in the side-lobes that the original synthetics show, leading to over-estimated peak amplitudes. Additionally, the trough of the waveform is over-estimated at all arrays except the farthest at 5 km.

Error Analysis

To summarize and compare the differences in fit between the synthetic and azimuthally symmetric synthetic waveforms we calculated the RMS error for each synthetic waveform as compared to the observed data (Fig. 14).

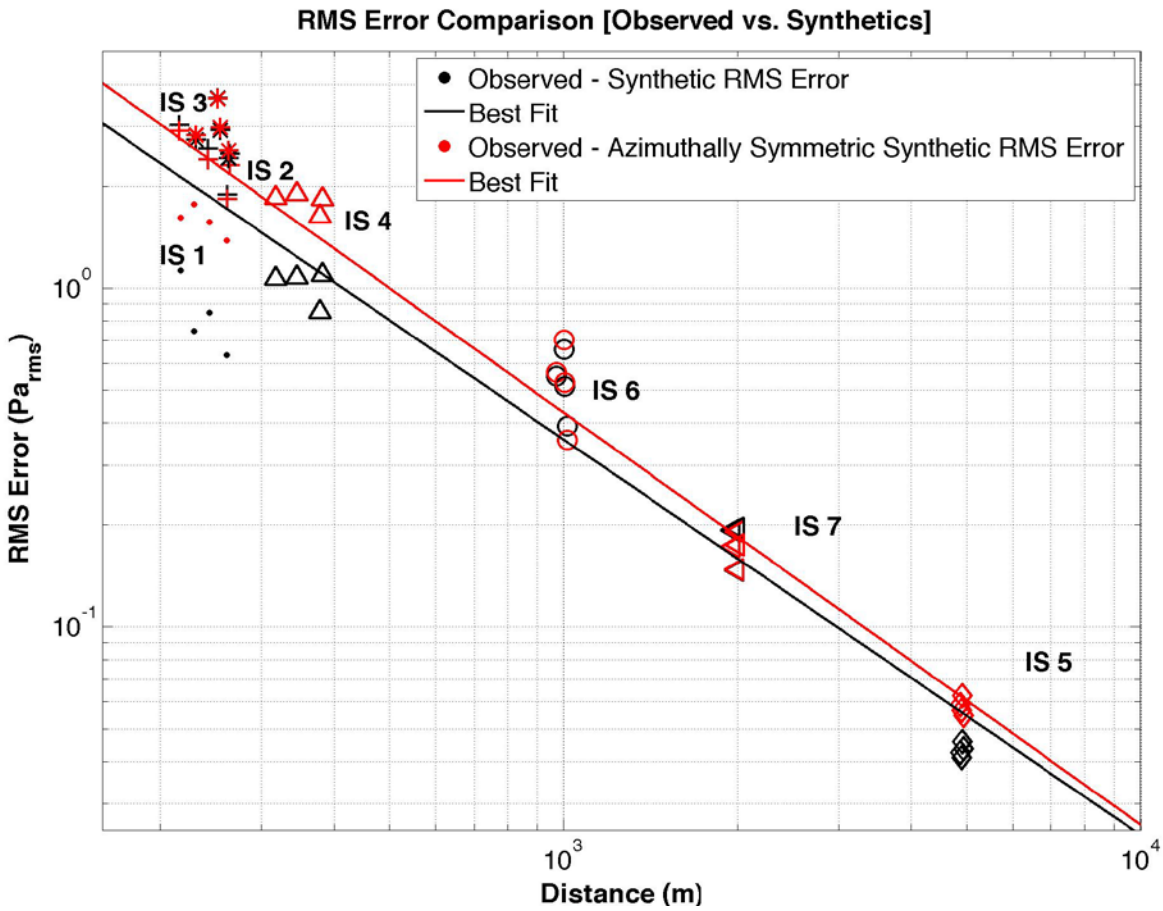

Figure 14. RMS Error comparison between the observed waveforms and the asymmetric synthetic waveforms (Black) and the observed waveforms and the symmetric synthetic waveforms (Red). Trend lines are fit to each comparison set.

The RMS error, in general, is higher for the azimuthally symmetric synthetic comparisons at all arrays except IS 2 and components of 3, 7 and 5. This corroborates what can be seen visually when comparing both synthetic data sets to the observed data. What is not immediately clear is why the azimuthally symmetric model more closely matches the observed data at IS 2. Further investigation is necessary to fully understand this anomaly, but may be related to the period of the signal. Fig. 15 summarizes the data from Fig. 14 by

showing only the difference in RMS between the two models at each array station. Positive values indicate that the azimuthally symmetric waveforms reproduced the observed data better than the original synthetics, while the negative values indicate the opposite. Again, for all array stations other than IS 2, the original synthetics either out-performed, or were very similar to the azimuthally symmetric synthetics.

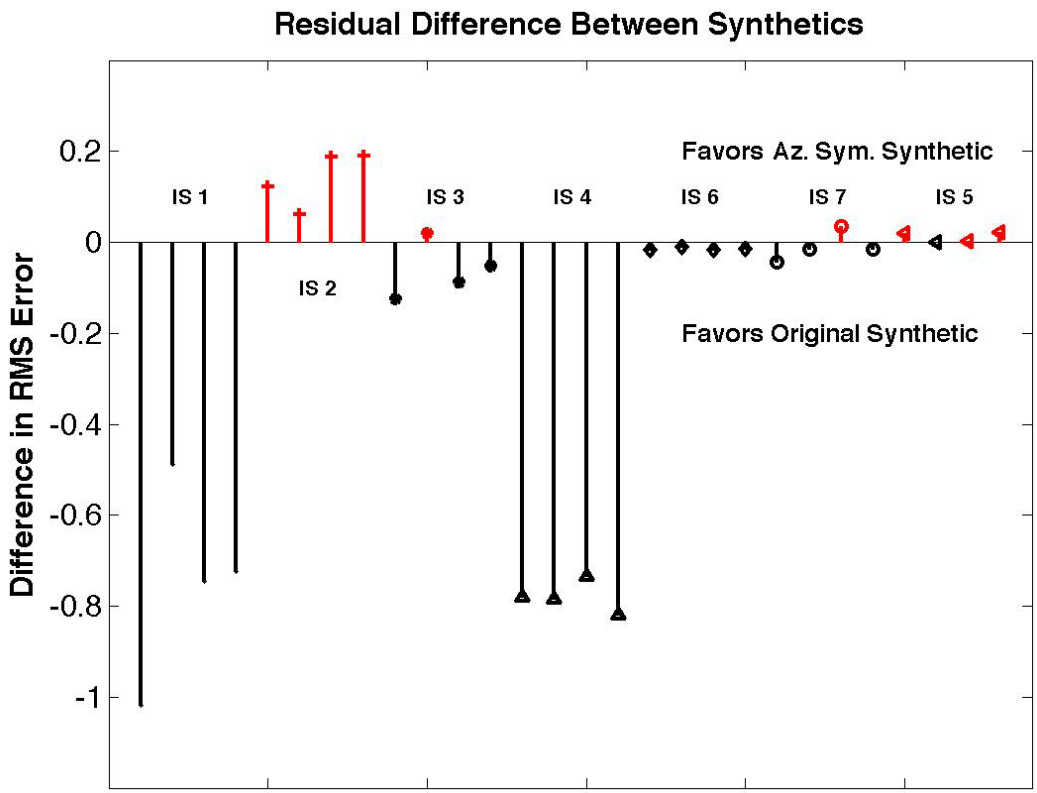

Figure 15. Difference in RMS error between the original synthetics and the azimuthally symmetric synthetics as compared to the observed data. Positive values indicate that the azimuthally symmetric synthetic waveforms have less error than the original synthetics, while a negative value indicates that the original synthetics have lower error.

Time-Domain, Finite-Difference Code: Caveat

For a separate computational approach, we have applied the time-domain, finite-difference code, Caveat, to the generation of the near field infrasound signal from the SPE2 event. Caveat is an established computational fluid dynamics (CFD) tool that has been applied to a variety physical problems involving both high speed and low speed flows. Caveat is documented in (Adessio et al. 1992). Quoting from part of the abstract in the (Adessio et al 1992) report below:

> CAVEAT uses an explicit time-marching, conservative finite-volume numerical technique in which all state variables, including velocity, are cell centered; values at vertices and cell faces are derived. The technique is a variation of the Godunov method that uses an approximate Riemann solver and accommodates arbitrary equations of state.

The advantage of a CFD code is that one gets a full wave solution in the full computational 2D domain but with longer computational times. Our calculations used two-dimensional cylindrical geometry with r,z coordinates. Boundary conditions at top and right are outflow boundaries and the left is the axis of symmetry. For our SPE application we use the applied velocity boundary condition at the bottom boundary, where the velocities are derived from the modeled accelerations based on the SPE-2 data. The velocity is only applied in radial extent out to the distance of sensible motion, ~ 90 m. Otherwise the bottom boundary is rigid. The velocities were derived from the model accelerations described earlier. We employed a grid of 2000 by 2000 cells with uniform 2 m zone size. These calculations were carried out to 10 seconds in problem time, when the signal is out to ~3 km distance.

Fig. 16 shows pressure contours in the air, at one-second intervals, showing the evolution of the signal. Two different ranges of contour levels are shown to highlight details early in

time and then later in time. Signal levels along the ground are falling rapidly by 10 seconds. The figure shows that the largest signal levels are at an elevation angle of ~45 degrees. We show in Fig. 17 a horizontal slice through the Caveat mesh through the first row of cells at 6 and 10 seconds. The signal features are close to those from the RI technique shown earlier.

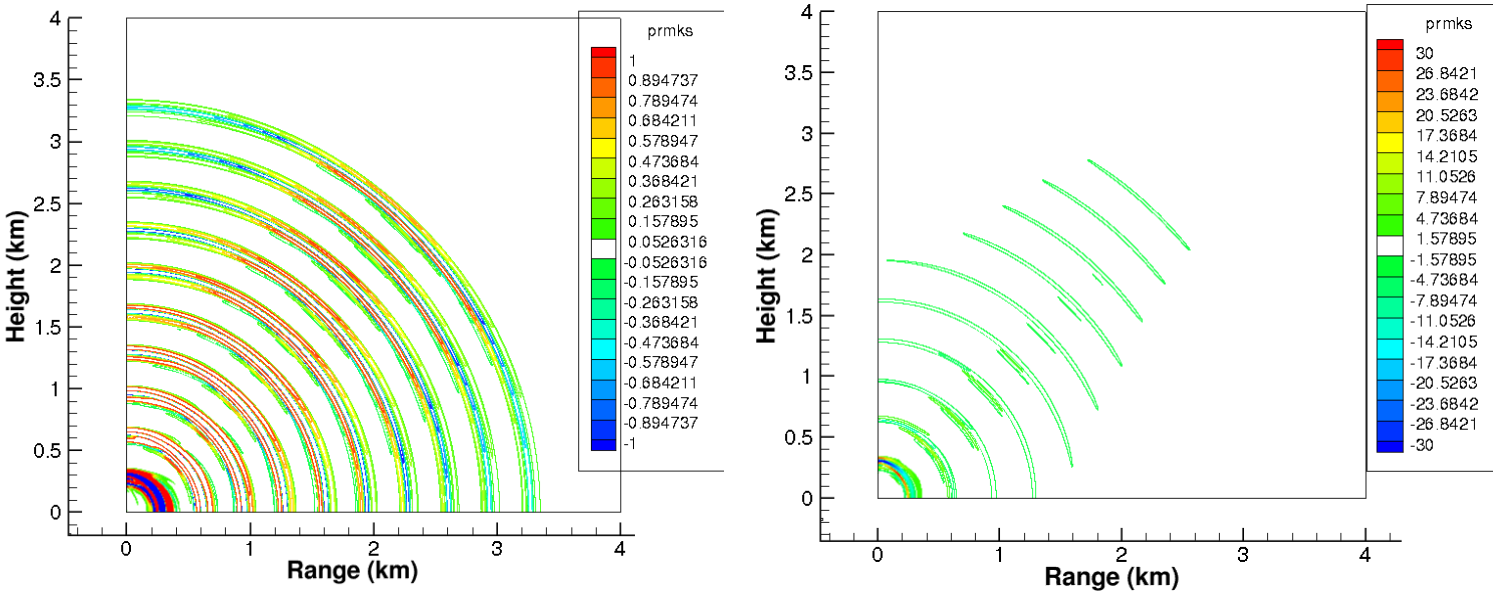

Figure 16. Pressure contours from the Caveat code at one second intervals. The left plot has contour values from ± 1 Pa to show more detail early in time. The right plot has contour values from ± 30 Pa to show detail in the later, weaker signal.

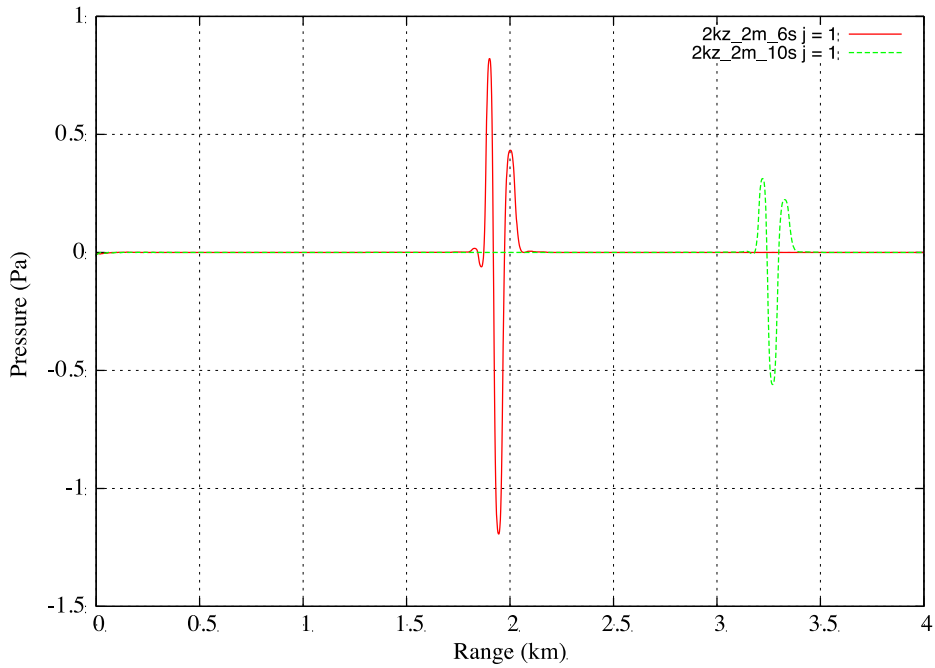

Figure 17. Pressure vs. range in the first horizontal row of cells in the Caveat mesh at 6 seconds (red) and 10 seconds (green).

Discussion and Conclusions

The repeated nature for SPE provides an excellent opportunity to study the infrasound generation from underground explosives tests in a controlled and highly instrumented environment. The "close-in" deployment of infrasound arrays and other multidisciplinary technologies, such as surface accelerometers, enables detailed modeling of the source region. Specifically, variations in the geology between the explosive source and the free surface lead to an asymmetric acoustic source that can be detected with a network of infrasound arrays.

We demonstrate that the Rayleigh integral can be used to produce synthetic pressure waveforms from a large distributed source region using a sparse network of surface accelerometers as an input source. While the overall shape, amplitude and asymmetry of the resulting synthetic waveforms is similar to the observed waveforms, an error analysis study between the asymmetric and azimuthally symmetric sources suggests that there is a portion of the source that is not being reproduced accurately in all cases around ground zero. It is important to note that the relative RMS errors between both models were small such that rotating one line of accelerometers around ground zero came very close to reproducing the observed data. In addition, it is possible that the asymmetric model does not represent the true extent of the ground motion and there may be other, non-vertical, components of the ground motion that couple to the atmosphere to produce the observed waveforms in such a way that neither the azimuthally symmetric model nor the original model accurately capture all of the physics involved. Furthermore, both the infrasound array geometry and the surface accelerometer locations are not optimal to completely define and capture the extent of the ground-to-air coupling. All but two of the infrasound arrays are below the elevation of the ground zero and the surface accelerometer placements are sparse, making the reconstruction of the source non-trivial.

However, we conclude that it is possible to accurately model the surface-to-air coupling of ground motion into the atmosphere from underground explosions using a sparse network of accelerometers and infrasound sensors using the Rayleigh integral technique. Furthermore, we have validated the results of the RI by utilizing a full-waveform, time-domain, finite-difference code (CAVEAT) to produce similar results.

Future work will include data from future SPE tests as well as models that are based on a completely synthetic source term instead of surface accelerometer data as well as adapting the Rayleigh code to deal with terrain specific sensor installations. Additionally, both the infrasound array network and surface accelerometers will be reconfigured and installed to better capture the subtle variations of the source in phase two of the SPE series of tests.

Acknowledgements

The authors want to thank Bobby Corbell (Sandia – Ret.) for deploying and collecting this data set as well Bob White and Ryan Emmitt (NSTec) for their invaluable and continued field efforts in support of this project. We would also like to thank Maggie Townsend (NSTec) for her valuable insight into the geology and surface fracturing of the SPE source region. Sandia National Laboratories is a multi-program laboratory managed and operated by Sandia Corporation, a wholly owned subsidiary of Lockheed Martin Corporation, for the U.S. Department of Energy's National Nuclear Security Administration under contract DE-AC04-94AL85000. SAND2013-9173J.

References

Addessio, F. L., Baumgardner, J. R., Dukowicz, J. K., Johnson, N. L., Kashiwa, B. A., Rauenzahn, R. M. & Zemach, C., 1992. CAVEAT: A Computer Code for Fluid Dynamics Problems with Large Distortion and Internal Slip, Los Alamos National Laboratory Technical Report, LA-10613-, Rev. 1.

American National Standards Institute, 1983. Airblast characteristics for single point explosions in air, ANSI Standard S2.20-1983, Acoustical Society of America, New York.

Arrowsmith, S. J., Burlacu, R., Pankow, K., Stump, B., Stead, R., Whitaker, R. & Hayward, C., 2012. A seismoacoustic study of the 2011 January 3 Circleville earthquake, Geophys. J. Int., 189, 1148-1158.

Banister, J. R., 1979. A program for predicting ground motion induced air pressures, SAND 78-2361, Sandia National Laboratories, Albuquerque, NM.

Blackstock, D. T., 2000. Fundamentals of Physical Acoustics, p. 541, John Wiley and Sons, New York

Chiokov, A, 2006. Scattered Data Interpolation and Approximation using Radial Base Functions, http://www.mathworks.com/matlabcentral/fileexchange/10056, MATLAB Central File Exchange. Retrieved May 1, 2012.

Christie D. R. & Campus, P., 2010. The IMS Infrasound Network: Design and Establishment of Infrasound Stations, in: Infrasound Monitoring for Atmospheric Studies, ed. By A. Le Pichon, E. Blanc and A. Hauchecorne, Springer, p. 29-76, doi: 10.1007/978-1-4020-9508-5.

Drellack, S. L., Prothro, L. B. & Reed D. N., 2011. Source Physics Experiment 2 Test Crack Mapping. National Security Technologies, LLC, Las Vegas, NV.

Drellack, S. L., Gonzales J. L. & Prothro, L. B., 2012. Geologic Surface Effects Mapped Following Source Physics Experiment 3. National Security Technologies, LLC, Las Vegas, NV.

Evers, L. G., Van Geyt, A., Smets, P. & Fricke, J., 2012. Anomalous infrasound propagation in a hot stratosphere and the existence of extremely small shadow zones, J. Geophys. Res., doi: 10.1029/2011JD017014, in press.

Hart, D. M., 2007. Evaluation of Inter-Mountain Labs Infrasound Sensors July 2007, Sandia National Labs Technical Report, SAND2007-7020, Albuquerque, NM.

Lee, H. & Walker J. J., 1980. Model for ground motion and atmospheric overpressure due to underground nuclear explosions, Los Alamos Scientific Laboratory Report. LA-8554-MS.

Morse, B. S., Yoo, T. S., Rheingans, P., Chen, D.T. & Subramanian, K. R., 2005. Interpolating implicit surfaces from scattered surface data using compactly supported radial basis functions, *ACM SIGGRAPH courses, ACM, 2005, pp. 78-87 doi: 10.1145/1198555.1198645.*

Snelson, Catherine M. et al., 2013. Chemical Explosion Experiments to Improve Nuclear Test Monitoring, *EOS,* **94,** Num. 27, p 237.

Szuberla, C. A. L., Arnoult, K. M. & Olson, J. V., 2006. Discrimination of near-field infrasound sources based on time-difference of arrival information, J. Acoust. Soc. Am. 120, EL20-EL28.

Whitaker, R., 2007. Infrasound Signals as Basis for Event Discriminants, in Proceedings of the 29th Monitoring Research Review: Ground-Based Nuclear Explosion Monitoring Technologies, LA-UR-07-5613, Vol. 1, pp. 905-913. http://www.osti.gov/bridge/product.biblio.jsp?osti_id=1027449

Whitaker, R., 2008. Infrasound Signals from Ground Motion Sources, in Proceedings of the 30th Monitoring Research Review: Ground-Based Nuclear Explosion Monitoring Technologies, LA-UR-08-05261, pp 912-920. http://www.osti.gov/bridge/product.biblio.jsp?osti_id=960561

Whitaker, R., 2009. Infrasound Signals from Ground Motion Sources, in Proceedings of the 30th Monitoring Research Review: Ground-Based Nuclear Explosion Monitoring LA-UR-09-05276, pp 750-758. http://www.osti.gov/bridge/product.biblio.jsp?osti_id=992203